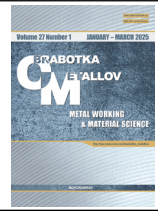




Obrabotka metallov -

Metal Working and Material Science

Journal homepage: http://journals.nstu.ru/obrabotka_metallov







Improvement the manufacturing quality of new generation heat-resistant nickel alloy products using wire electrical discharge machining

Evgeniy Shlykov ^{a, *}, Timur Ablyaz ^b, Vladimir Blokhin ^c, Karim Muratov ^d

Perm National Research Polytechnic University, 29 Komsomolsky prospekt, Perm, 614990, Russian Federation

^a  <https://orcid.org/0000-0001-8076-0509>,  Kruspert@mail.ru; ^b  <https://orcid.org/0000-0001-6607-4692>,  lowrider11-13-11@mail.ru;

^c  <https://orcid.org/0009-0009-2693-6580>,  warkk98@mail.ru; ^d  <https://orcid.org/0000-0001-7612-8025>,  Karimur_80@mail.ru

ARTICLE INFO

Article history:

Received: 12 December 2024

Revised: 19 December 2024

Accepted: 28 December 2024

Available online: 15 March 2025

Keywords:

Wire electrical discharge machining

Surface roughness

Accuracy

Microcracks

Surface layer

Cyclic testing

Funding

The research was financially supported by the Russian Science Foundation grant No. 23-79-01224, <https://rscf.ru/project/23-79-01224/>.

ABSTRACT

Introduction. The paper presents the results of an experimental study on the quantitative and qualitative evaluation of the surface after wire electrical discharge machining (*WEDM*). **The purpose of this study** is an experimental investigation with qualitative and quantitative analysis of surface defects in samples made of a heat-resistant nickel alloy *VV751P* after *WEDM*. **Methods of research.** Samples for the study with a specific geometry were obtained by the wire electrical discharge machining method in 4 modes. The operating parameters were: workpiece height (h , mm), pulse-on time (T_{on} , μ s), and pulse-off time (T_{off} , μ s). The samples were studied using a *Hitachi S-3400N* electron microscope in backscattered electron mode at 25 kV. Surface topography after electrical discharge machining was evaluated using a laser scanning microscope (*LSM LextOLS4000*). Cyclic tests were performed on a universal testing machine *Biss-00-100* at a test frequency of 20 Hz in a symmetrical cycle ($R = -1$). **Results and discussion.** The defective (white) layer of samples was analyzed. It is established that during wire electrical discharge machining the thickness of defective white layer is within 10 μ m, both after processing in minimum and maximum mode. The surface quality index (surface roughness Ra) was analyzed. It was found that the average value of surface roughness parameter Ra is 1.62 μ m when processing samples with a height of 10 mm. When the sample height increases, the surface roughness value reaches 2.6 μ m after processing in minimum mode and 3.4 μ m after processing in maximum mode. It is established that with an increase in workpiece height, the number of microcracks on the surface of the product increases, which is associated with the intensification of the interaction of single pulses with the processed surface. As a result of the study, it is found that at a loading amplitude of 400 MPa, an average value of the number of cycles reaches $1.50E + 05$ cycles. A decrease in the number of cycles is observed with an increase in the amplitude of the loading cycles.

For citation: Shlykov E.S., Ablyaz T.R., Blokhin V.B., Muratov K.R. Improvement the manufacturing quality of new generation heat-resistant nickel alloy products using wire electrical discharge machining. *Obrabotka metallov (tehnologiya, oborudovanie, instrumenty)* = Metal Working and Material Science, 2025, vol. 27, no. 1, pp. 34–47. DOI: 10.17212/1994-6309-2025-27.1-34-47. (In Russian).

Introduction

Modern industry faces constant requirements for product quality. The introduction of new-generation alloys results in increased physical and mechanical properties of products. For example, the introduction of the granulated, heat-resistant nickel alloy *VV751P* into production has led to increased stability of aviation products in high-temperature environments without sacrificing their mechanical properties. Products made of heat-resistant alloy *VV751P* offer extended service life and improved cyclic durability [1-3].

The modern aircraft engine building industry predominantly uses machining for manufacturing products. Introducing new materials significantly complicates the serial production process. Heat-resistant materials' machining presents several technological and economic disadvantages. The high hardness of heat-resistant alloys causes build-up on the cutting tool, reducing tool durability and lowering machining accuracy. Other

* Corresponding author

Shlykov Evgeniy S., Ph.D. (Engineering), Associate Professor
 Perm National Research Polytechnic University,
 29 Komsomolsky prospekt,
 614990, Perm, Russian Federation
 Tel.: +7 961 759-88-49, e-mail: Kruspert@mail.ru

challenges in machining by cutting include hardening and the low thermal conductivity of the material being machined. During the cutting process, a significant amount of heat is generated, intensifying and localizing thermal effects on the cutting edge and accelerating tool wear [4-5].

Wire-cut electrical discharge machining (*WEDM*) is an alternative method for manufacturing new-generation, heat-resistant alloys [6-10]. *WEDM* relies on removing material from the workpiece surface through heat generated by electrical impulses between the tool-electrode (*TE*) and the workpiece-electrode (*WE*). This process is independent of the material's mechanical strength, hardness, toughness, and brittleness. There is no mechanical impact on the surface being processed [11-14].

When implementing *WEDM* in production, it is essential to investigate surface quality assurance during machining. In *WEDM*, short-time unit pulses create intense, localized thermal and chemical effects on the workpiece surface. This forms an outer surface layer with physical and mechanical properties that differ from those of the base material. This layer may exhibit hardness values that differ from the base material and may contain cracks and other surface defects. The energy of each pulse and its duration determine the thickness of the modified layer.

In addition to surface defects, residual stresses are also intensified in this layer. The intense thermal influence can cause residual stresses to appear in the surface layer of the workpiece. The magnitude and direction of these stresses depend directly on the processing modes, the material's physical and chemical properties, and the surface layer characteristics [15-18].

To minimize the thickness of the modified surface layer, it is necessary to study the influence of machining modes on the formation of this layer [19-21]. Machining modes affect the surface quality indicator, *Ra* (roughness).

After *WEDM*, inhomogeneities can be observed in the surface relief, which is formed by the superposition of numerous craters. These craters result from the impact of unit pulses on the workpiece surface. The surface microrelief after *WEDM* differs from surfaces obtained by blade tool.

The actual purpose is to provide surface quality at machining of heat-resistant nickel alloys of new generation by wire-cut electrical discharge machining.

The purpose of this work is an experimental investigation with qualitative and quantitative analysis of the analysis of defects on the surface of samples made of a heat-resistant nickel alloy *VV751P* after *WEDM*.

Objectives:

- to analyze the thickness of the defective layer (white layer) on samples of the heat-resistant alloy *VV751P* manufactured in this study.
- to analyze the surface quality indicator, *Ra* (μm), of the manufactured samples.
- to conduct surface investigations for microcracks and structural defects using a laser scanning microscope and evaluate the temperature effect on the formation of the surface microrelief.
- to conduct cyclic fatigue tests on specimens made of the heat-resistant alloy *VV751P* after *WEDM*.

Research methodology

The experiments were conducted at the *Center of Additive Technologies* of the ITM Department of the Perm National Research Polytechnic University. During the experiments the samples shown in Fig. 1 were produced. Wire-cut electrical discharge machining (*WEDM*) was performed using an *Electronica EcoCut* machine manufactured by *ElectronicaMachineTools* (Pune, India). Throughout the study, *BercoCut* wire manufactured by *Berkenhoff GmbH* (Herborn, Germany) with a diameter of 0.25 mm was used as the tool-electrode. Distilled water served as the working medium to facilitate the machining process.

The samples were machined using minimum and maximum modes. Each experiment was repeated three times to exclude the appearance of random errors. The pulse on-time (T_{on} , μs), pulse off-time (T_{off} , μs), and sample height were selected as the variable machining parameters. The modes of *WEDM* are presented in Table 1.

The surface roughness of the machined samples after *WEDM*, in terms of the *Ra* parameter, was measured using a *Perthometer S2* profilometer (Mahr GmbH, Göttingen, Germany) with a base trace length of 0.8 mm.

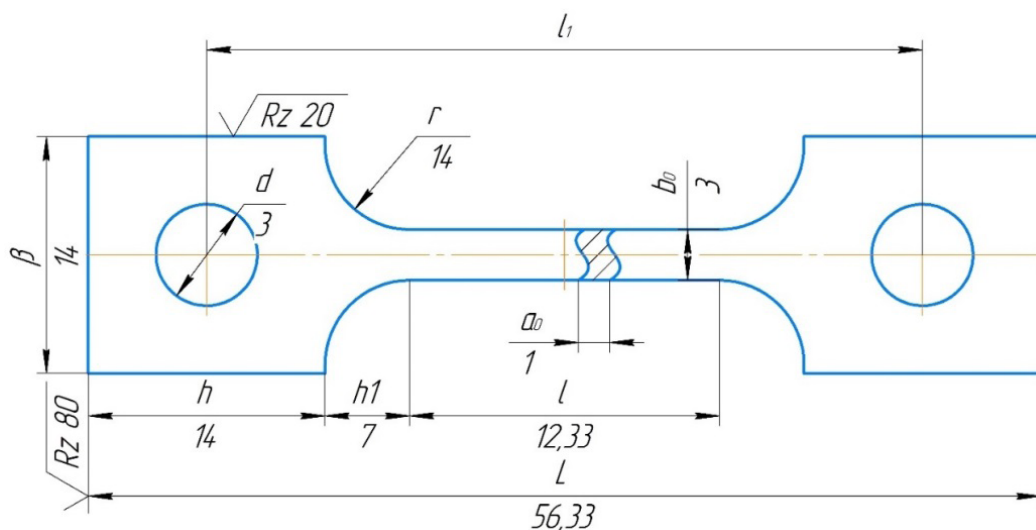


Fig. 1. Specimen geometry

Table 1

WEDM modes

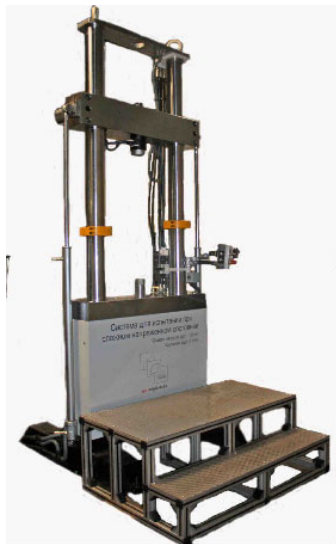
Mode No.	$T_{on}, \mu s$	$h, \mu s$	$T_{off}, \mu s$
1	21	10	60
2	30		
3	21	15	
4	30		

Surface topography after electrical discharge machining was obtained using a laser scanning microscope (LSM) *Lext OLS4000* (Olympus Corporation, Tokyo, Japan) based on a three-dimensional image model. The surface model was generated using the *3DRoughnessReconstruction* software module (Olympus Corporation, Tokyo, Japan). The three-dimensional surface was constructed from optical slices acquired through *X-Y-Z* scanning of specific surface areas. Scanning was performed at $\times 200$ and $\times 1,000$ magnifications, with a scanning step of $2 \mu m$ along the *Z*-axis. A semiconductor laser with a wavelength of 405 nm served as the light source for scanning. For visual evaluation of the processing results, a *Hitachi S-3400N* scanning electron microscope was used in backscattered electron mode at a voltage of 25 kV .

Cyclic tests were performed on a *Biss-00-100* universal testing machine (Fig. 2, a) at a test frequency of 20 Hz in a symmetrical cycle ($R = -1$). Fatigue testing was controlled using a soft loading method, which involves a smooth and controlled increase in applied stresses. Three key factors, carefully monitored by specialized measuring equipment, served as criteria for test termination. The test was terminated when the specimen failed completely - the most obvious indication that the material's endurance limit had been reached. The test was also terminated upon reaching a predetermined number of loading cycles, a multiple of $100,000$. This parameter reflects the accumulation of plastic strain in the material. A test termination occurred when the strain range increased by more than 20% from the initial value. Exceeding the acceptable 20% threshold signals a significant reduction in the specimen's load-carrying capacity and indicates impending failure. It is important to note that this threshold may vary depending on the material type and test conditions.

To investigate the influence of the surface *WEDM* process on fatigue characteristics, specimens were removed from tests after $100,000$ cycles. Optical surface scanning was performed using a *NewView 5010* optical profilometer (Fig. 2, b). This device enables the creation of a digital model of the surface relief and




a

b

Fig. 2. Equipment for studying the effect of cyclic tests on surface deformation:
a – Servo-hydraulic universal testing machine *Biss-00-100*; *b* – Interferometer-profilometer
NewView 5010

allows for both qualitative and quantitative analysis of the changes that occurred on the material's surface during the tests.

Results and Discussion

In this study, samples of heat-resistant nickel alloy *VV751P* produced by *WEDM* at minimum and maximum modes, were analyzed. The surface layer of the samples was evaluated qualitatively and quantitatively using an *Olympus GX51* optical microscope at $\times 200$ magnification (Fig. 3).

It was observed that, with *WEDM*, the size of the defective white layer remained consistent at both modes and was $10\ \mu\text{m}$. Varying the processing parameters within this range did not significantly impact the thickness of the defect layer.

Fig. 4 shows the surface of a heat-resistant nickel alloy *VV751P* sample processed by *WEDM* at the minimum mode (Mode No.1). Scanning electron microscopy (SEM) revealed no surface defects in the form of pores or cracks. During the *WEDM* process, spark discharges occur, and a microvolume of molten

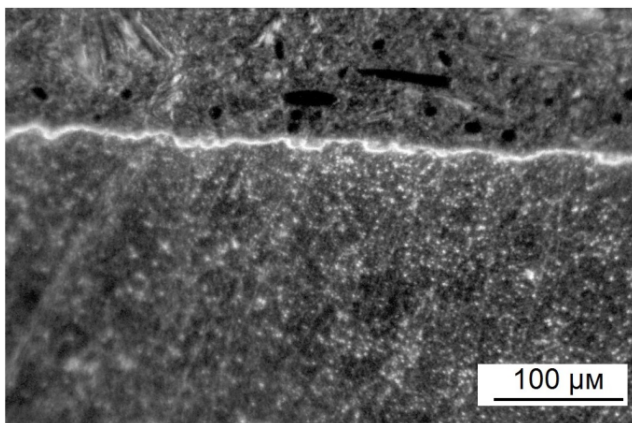
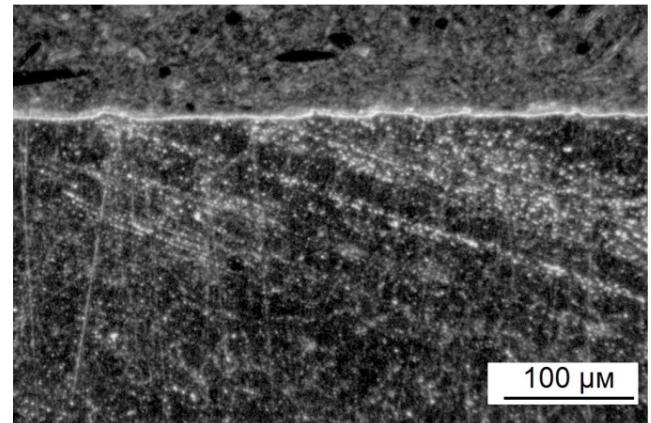

a

b

Fig. 3. Structure of the surface layer of *VV751P* samples after *WEDM* in:
a – minimum mode; *b* – maximum mode

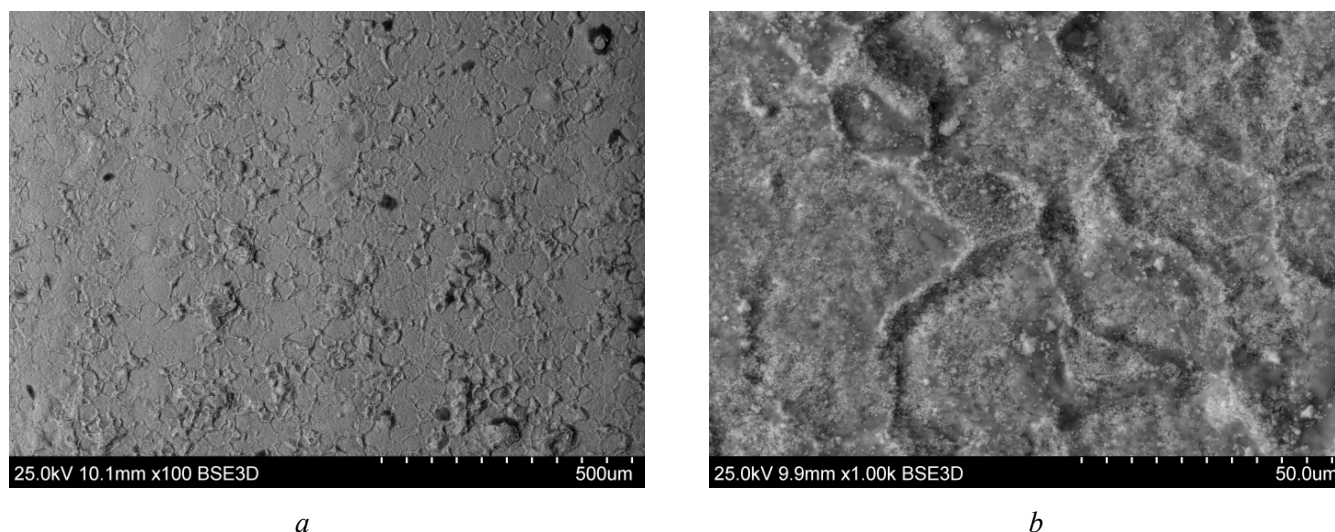


Fig. 4. Surface of the specimen made of heat-resistant nickel alloy *VV751P* after *WEDM* according to mode No. 1, obtained using *SEM*:

a – 100× magnification; *b* – 1,000× magnification

metal is ejected from the sample, resulting in the formation of a microcrater. The ejected molten metal rapidly solidifies, forming a characteristic bead around the crater's perimeter. Figs. 4, *a* and 4, *b* show no pronounced zones of melt in the form of craters, beads, depressions, or sharp peaks.

Fig. 5 shows the surface topography of the sample after processing in mode No. The average surface roughness (Ra) was 1.53 μm .

Examination of the sample surface, machined according to mode No.1, using a confocal scanning laser microscope (*CSLM*) *Lext OLS4000*, revealed a relatively flat surface with a characteristic microrelief formed by melting of the sample material during machining. No pores or cracks were observed on the processed surface.

With increasing pulse energy (mode No.2), an intensification of the material melting process was observed. The molten alloy spreads randomly across the surface, creating irregularities of different shapes and sizes. This process results in variations in the roughness of the surface layer. Due to the intense thermal impact on the workpiece surface layer during *WEDM*, secondary structures form on the surface. It has been established that increasing *WEDM* power in mode No.2, while maintaining the height of the machined sample at 10 mm, does not lead to significant qualitative changes in the overall surface morphology (Fig. 6, *a*). However, at higher magnifications (Fig. 6, *b*), microcracks are revealed on the processed surface. These microcracks likely formed during rapid cooling of the molten metal from elevated temperatures due to the more intense energy input compared to mode No.1. Fig. 6, *b* shows the presence of microcracks within the craters on the surface of a 10 mm high specimen machined in mode No.2.

Fig. 7 shows a representative section of the heat-resistant nickel alloy *VV751P* sample surface after machining in mode No.2. A less pronounced temperature gradient is observed compared to mode No.1. The average surface roughness (Ra) was determined to be 1.62 μm , which is consistent with the roughness value obtained in mode No.1, placing both surfaces within the same roughness class.

Increasing the height of the machined sample to 15 mm intensifies microcrack formation on its surface during *WEDM*, regardless of the machining power (Fig. 8, *a-f*). The effect of secondary discharges is illustrated in Fig. 8. The final stage is characterized by cavitation phenomena and a plasma luminous plume (with a characteristic lifetime of 5 ms) that exists due to the increased frequency of high-frequency discharges near the cathode. At the beginning of the third stage, vapor-gas layer bubbles begin to collapse due to the equilibration of internal and external pressure as a result of increasing local temperature, which is a derivative of the applied pressure. This leads to a large cavitation shock (approximately 1010 MPa), which further increases the surface roughness parameter and promotes the growth of technological cracks during *WEDM* of heat-resistant nickel alloy *VV751P*.

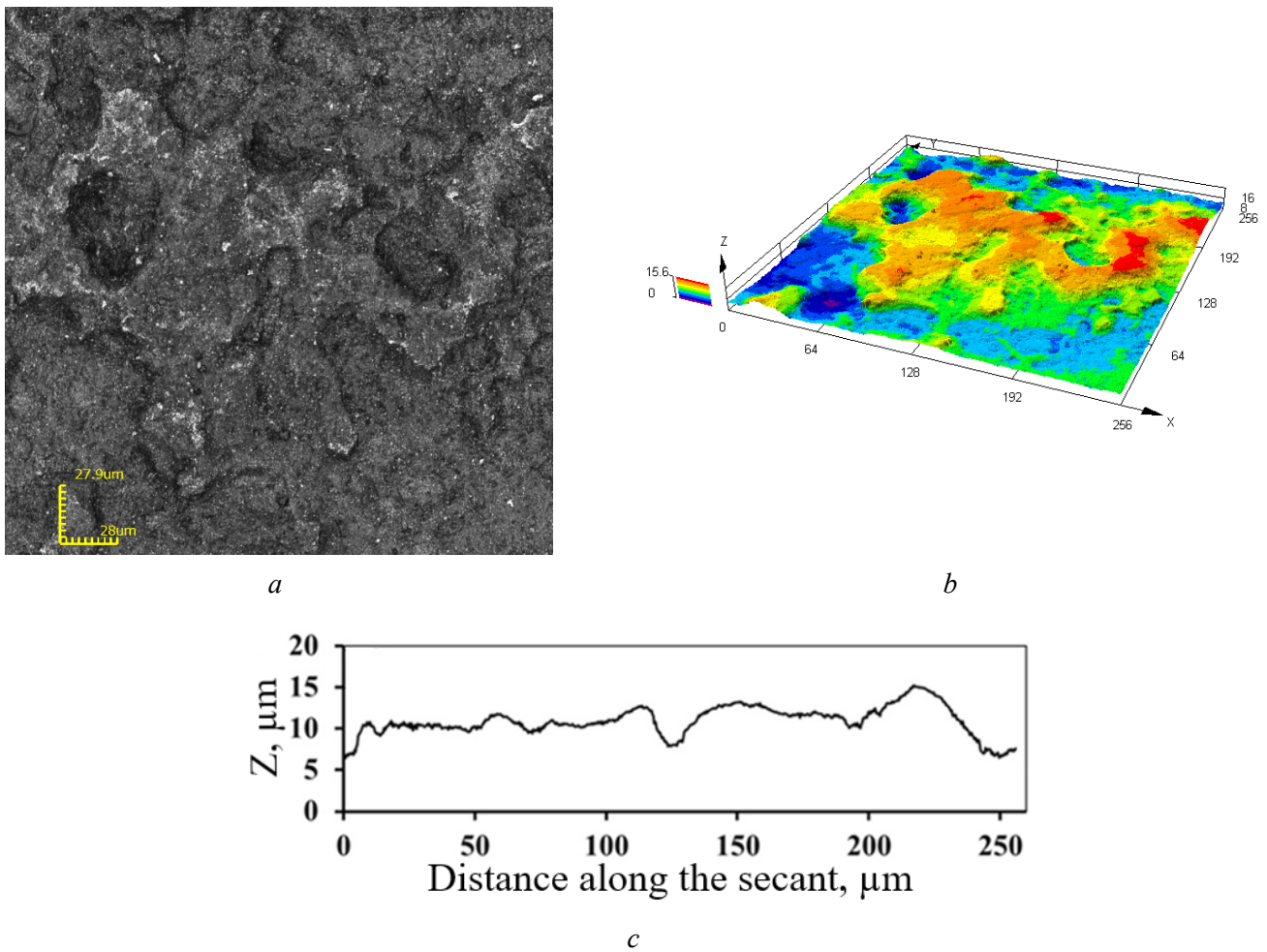


Fig. 5. CSLM at 500× magnification:

a – a random area of the sample surface after processing in mode No. 1 with a secant line; *b* – 3D model with a temperature map of heights; *c* – graph of microrelief variation along the secant line

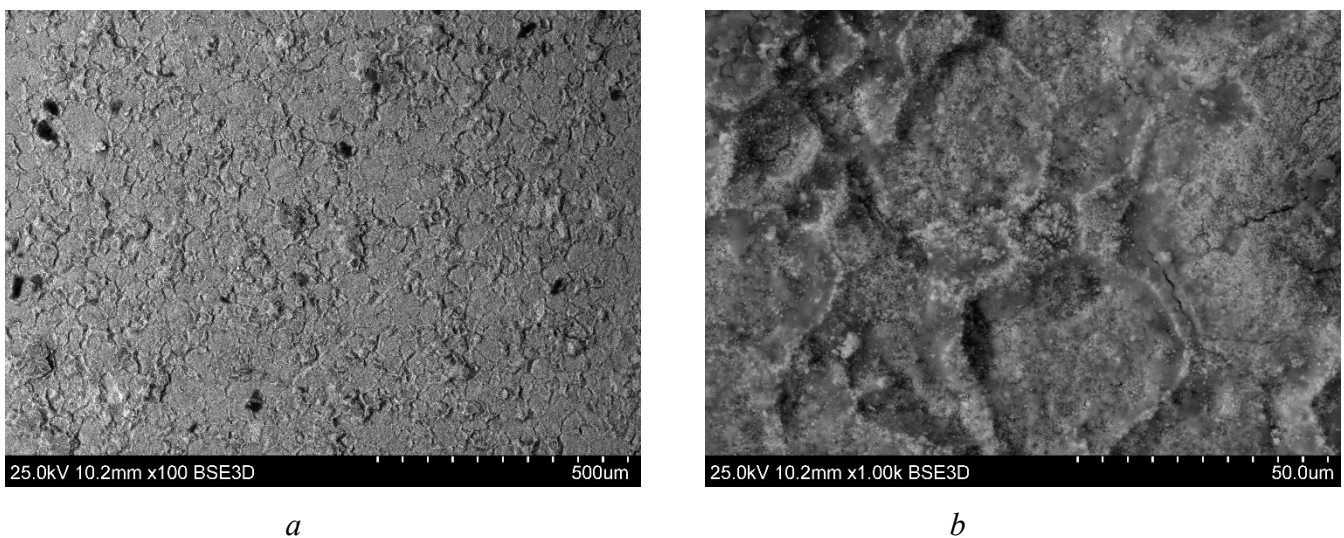


Fig. 6. Surface of the specimen made of heat-resistant nickel alloy *VV751P* after *WEDM* in mode No. 2, obtained using *SEM*:

a – at 100× magnification; *b* – at 1,000× magnification

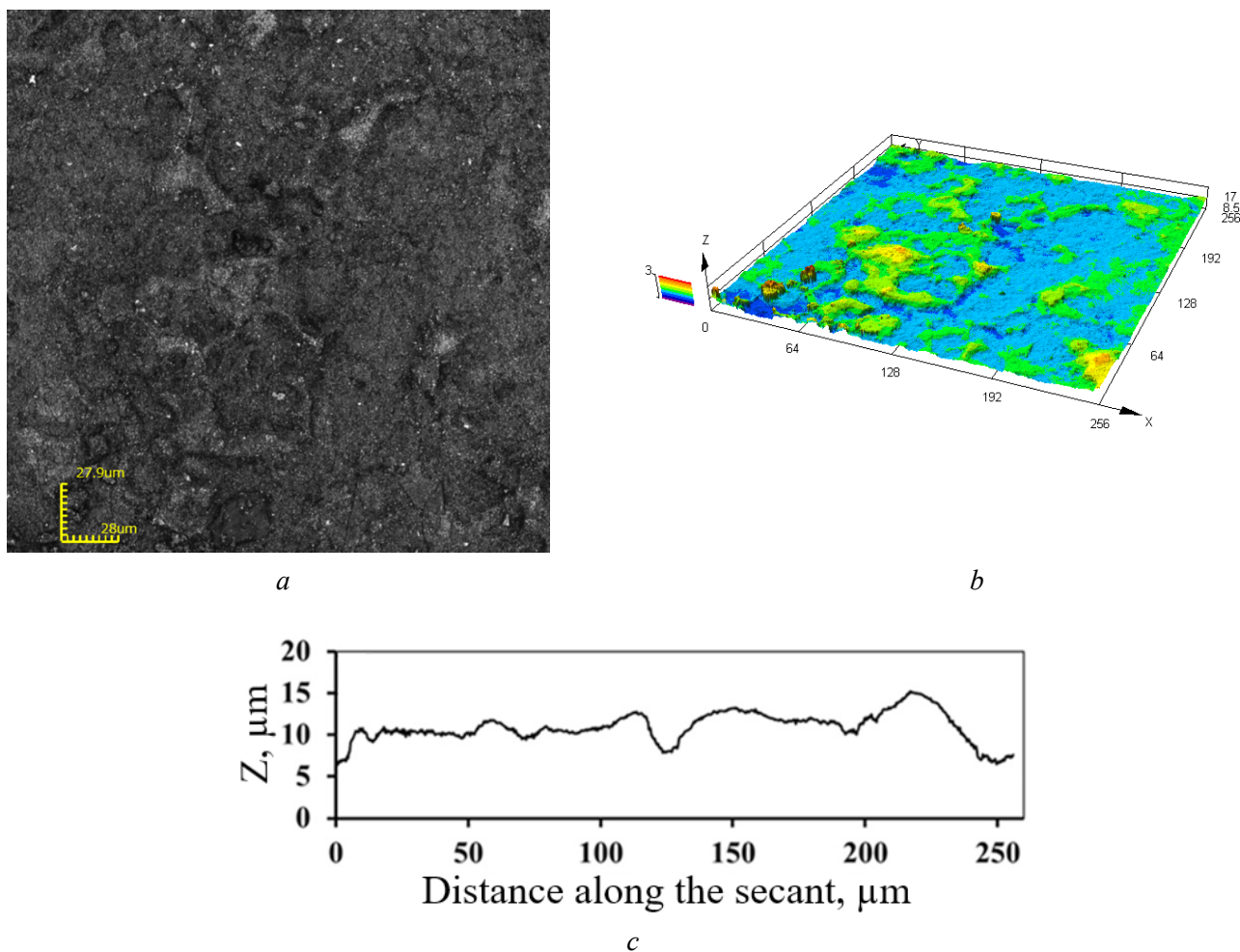


Fig. 7. CSLM at 500× magnification:

a – a random area of the sample surface after processing in mode No. 2 with a secant line; *b* – 3D model with a temperature map of heights; *c* – graph of microrelief variation along the secant line

As the pulse energy increases, process cracks resulting from *WEDM* are nucleated, in addition to increasing the surface roughness. Rapid heating of the workpiece to a temperature of 5,000 °C, followed by rapid cooling to the temperature of the distilled water (20 °C), promotes crack formation on the machined surface. This phenomenon is caused by thermal stresses that lead to cracking of the metal. An important factor affecting crack formation is the presence of depressions and holes, which act as stress concentrators.

After surface machining of a 15 mm high specimen in mode No.3, relatively large microcracks are detected by SEM even at relatively low magnifications (Fig. 8, *a*). At slightly higher magnifications, it becomes evident that microcracks on the machined surface, compared to the surfaces of 10 mm high specimens machined in modes No.1 and No.2, become deeper and more branched (Fig. 8, *c*). More detailed studies of the machined surface at ×5,000 magnification revealed fine crystalline formations of submicron size along the boundaries of which zigzag-shaped microcracks are observed, as indicated by arrows in Fig. 8, *d*.

No significant qualitative changes in the microrelief of the specimen surface with a height of 15 mm machined in mode No.3 were observed compared to the microrelief of the surface of the specimen with a height of 10 mm machined in mode No.2 (Fig. 9). The surface roughness parameter *Ra* after *WEDM* in mode No.3 was 2.6.

On the surface of the specimen machined in mode No.4, a significant number of cracks and cracking are also observed (Fig. 8, *b, d*). As shown by *CSLM* studies of the sample surface (Fig. 10), the depth of these cracks and cracking exceeds 1 μm. No macroscopic defects in the form of large pores or cavities were detected.

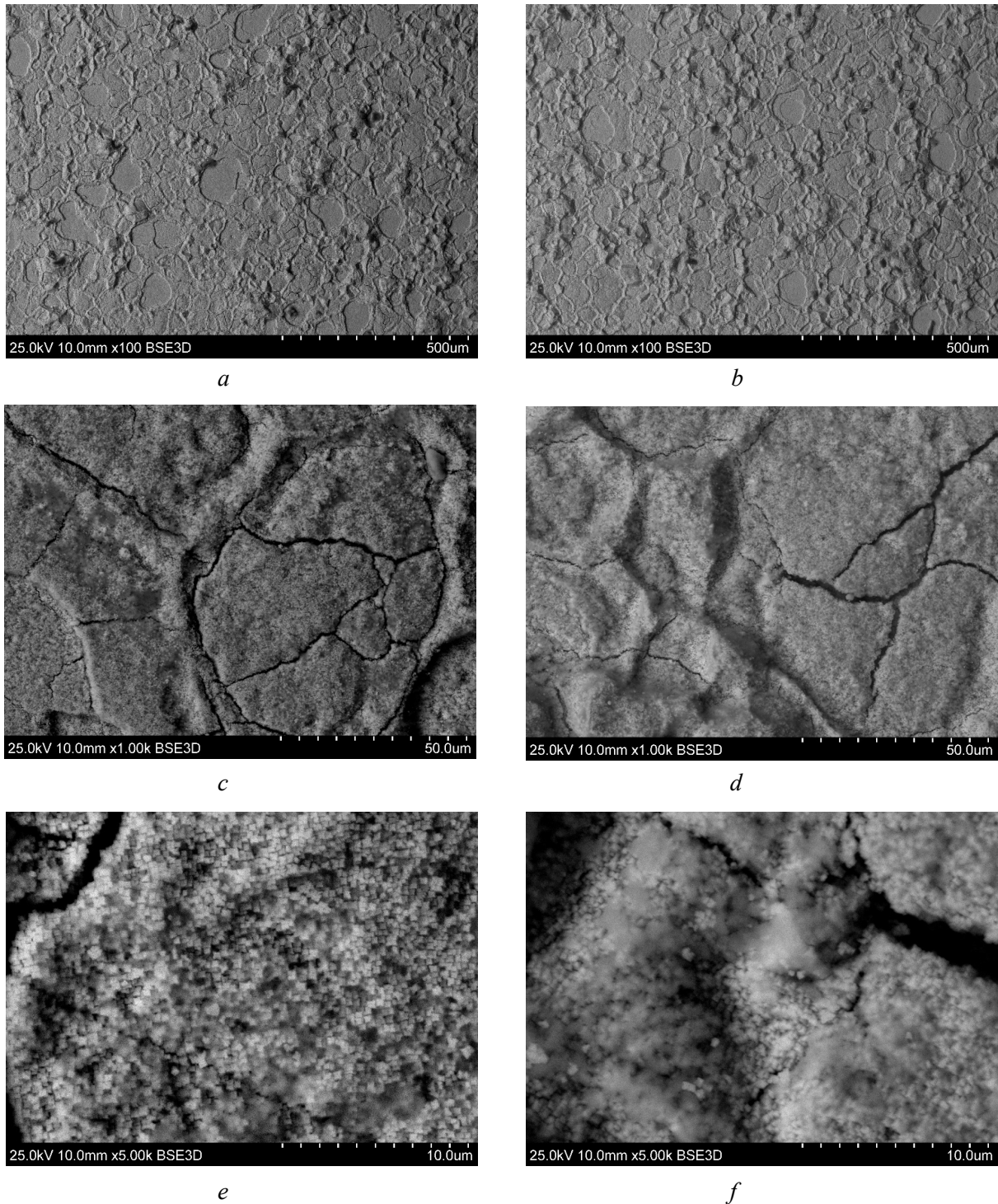


Fig. 8. Surface of samples made of heat-resistant nickel alloy *VV751P*, after *WEDM* in the mode: *a* – No. 3 at 100× magnification; *b* – No. 4 100× magnification; *c* – No. 3 1,000× magnification; *d* – No. 4 at 1,000× magnification; *e* – No. 3 at 5,000× magnification; *f* – No. 4 at 5,000× magnification (obtained by *SEM*)

The formation of microcracks and crazing in the sample machined by *WEDM* in mode No.3 is caused by the formation of fine crystalline structures during rapid crystallization from the melt at elevated temperatures. Increasing the height of the sample increases the exposure time of unit pulses, consequently intensifying the thermal effect. The resulting stresses cause the formation of microcracks, which can subsequently merge to form larger cracks. The surface roughness parameter *Ra* was 3.4 μm.

Increasing the height of the workpiece being machined leads to an increased concentration of energy on the machined surface, causing secondary discharge phenomena that negatively impact the concentration

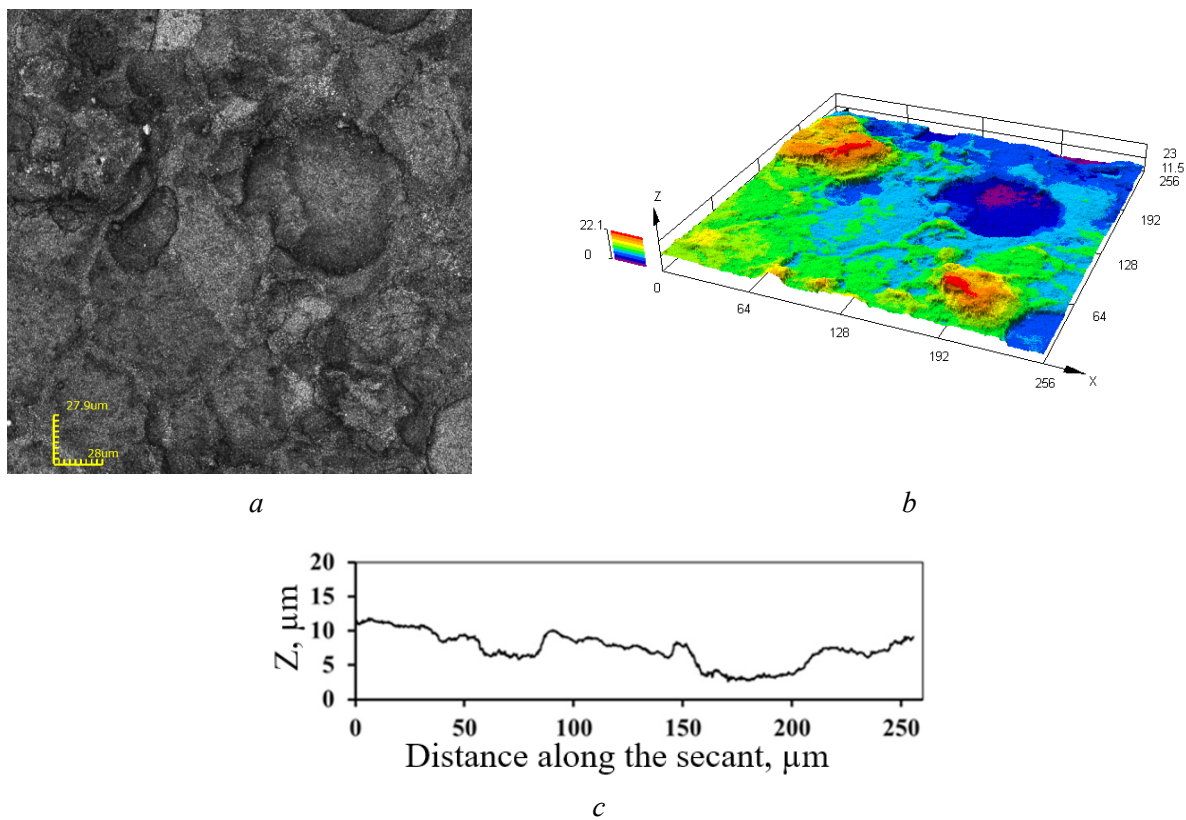


Fig. 9. CSLM at 500× magnification:
a – a random area of the sample surface after processing in mode No. 3 with a secant line;
b – 3D model with a temperature map of heights; *c* – graph of microrelief variation along the secant line

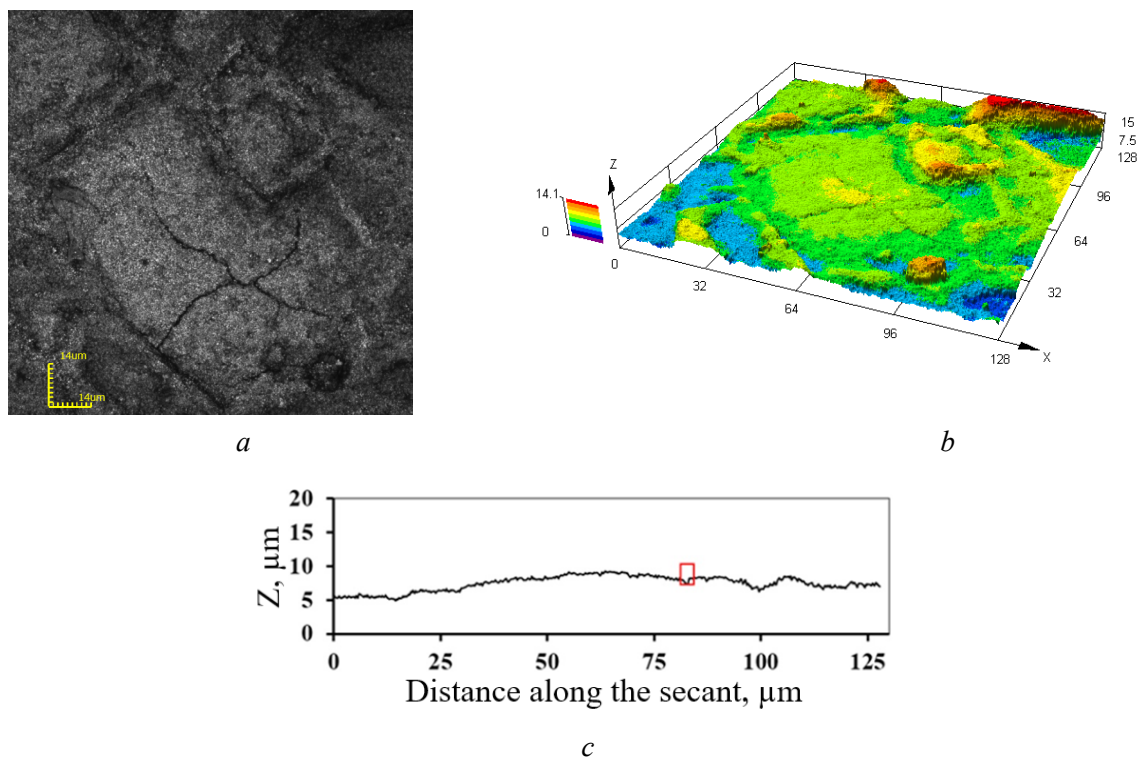


Fig. 10. CSLM at 500× magnification:
a – a random area of the sample surface after processing in mode No. 4 with a secant line; *b* – 3D model with a temperature map of heights; *c* – graph of microrelief variation along the secant line

and intensity of crack formation on the surface of heat-resistant nickel alloy *VV751P*. The presence of cracks on the surface negatively affects the performance of products made of heat-resistant nickel alloys.

Cyclic low-cycle fatigue tests were conducted to determine the time, nature, and mechanism of failure under cyclic loads on critical products made of functional materials. Low-cycle fatigue reflects failure under elastoplastic deformation of the product. The cyclic test data are shown in Table 2, and the fatigue diagram is shown in Fig. 11.

Table 2

Results of cyclic tests of *VV751P* alloy

Mode No.	stresses in the loading cycle		Number of cycles	Result
	kN	MPa		
1	0.75	263	2.50E+05	undestroyed
2	1	351	1.74E+05	destroyed
3	2	702	1.90E+04	destroyed
4	1.5	526	4.18E+04	destroyed
5	1.2	421	1.62E+05	destroyed
6	1.1	386	92700	destroyed

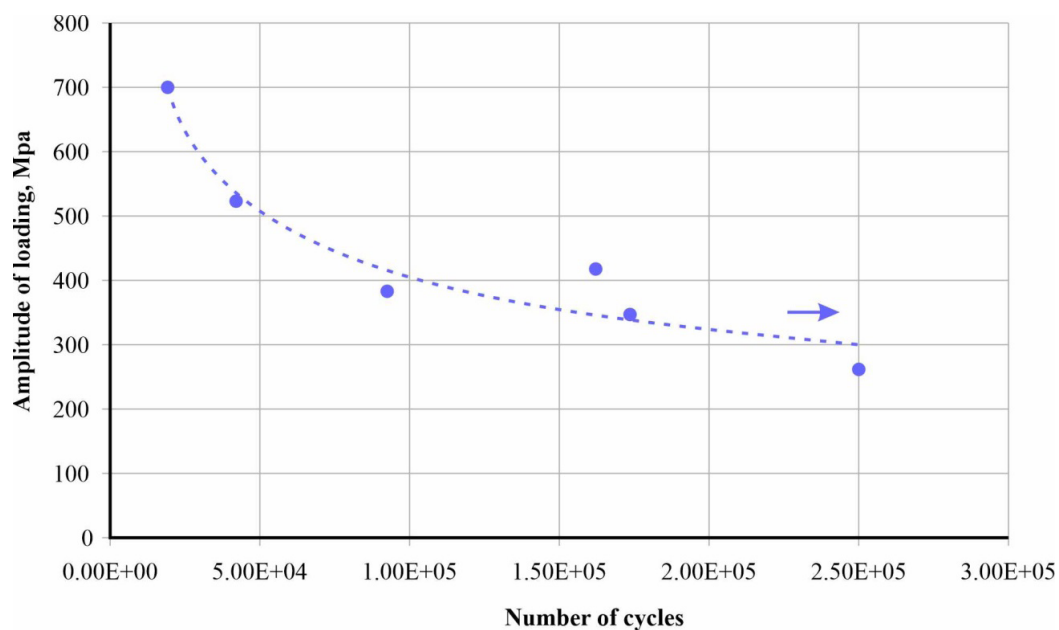


Fig. 11. Low-cycle fatigue diagram for the *VV751P* alloy (an arrow indicates a run-out sample that did not fracture after the specified number of cycles)

The study revealed that at a loading amplitude of 400 MPa, the average number of cycles to failure reached 1.50E+05 cycles. A decrease in the number of cycles to failure was observed with increasing loading amplitude. The arrow in the graph indicates the specimen that did not fail within the given number of cycles.

Conclusions

Analysis of the defective layer (white layer) of the samples revealed that the thickness of this layer remains consistent at approximately 10 μm after *WEDM*, regardless of the processing mode.



Analysis of the surface quality parameter, Ra (roughness), established that the average roughness (Ra) is 1.62 μm for machined samples with a height of 10 mm. Increasing the sample height causes the surface roughness to reach 2.6 μm at the minimum mode and 3.4 μm at the maximum mode.

It is established that increasing the workpiece height results in the formation of microcracks on the product surface, with the extent of cracking increasing at the maximum mode. Crack formation is attributed to the intensified interaction of unit pulses with the machined surface. Machining a 10 mm high sample showed no pores or cracks on the surface. Machining 15 mm high samples resulted in cracks on the surface, reaching lengths of up to 50–60 μm .

The study revealed that at a loading amplitude of 400 MPa, the average number of cycles reached 1.50E+05 cycles. A decrease in the number of cycles was observed with increasing loading amplitude.

References

1. Nowotnik A. Nickel-based superalloys. *Reference Module in Materials Science and Materials Engineering*, 2016, vol. 107 (2), pp. 1–6. DOI: 10.1016/B978-0-12-803581-8.02574-1.
2. Neumeier S., Freund L.P., Göken M. Novel wrought γ/γ' cobalt base superalloys with high strength and improved oxidation resistance. *Scripta Materialia*, 2015, vol. 109, pp. 104–107. DOI: 10.1016/j.scriptamat.2015.07.030.
3. Sommer D., Safi A., Esen C., Hellmann R. Additive manufacturing of Nickel-based superalloy: optimization of surface roughness using integrated high-speed milling. *Proceedings of SPIE*, 2024, vol. 12876. *Laser 3D Manufacturing XI*. DOI: 10.1117/12.3000972.
4. Inozemtsev A.A., Sandratsky V.L. *Gazoturbinnyye dvigateli* [Gas turbine engines]. Perm', Aviadvigatel' Publ., 2006. 1204 p.
5. Ho K.H., Newman S.T. State of the art electrical discharge machining (EDM). *International Journal of Machine Tools and Manufacture*, 2003, vol. 43 (13), pp. 1287–1300. DOI: 10.1016/S0890-6955(03)00162-7.
6. Rajurkar K.P., Sundaram M.M., Malshe A.P. Review of electrochemical and electrodischarge machining. *Procedia CIRP*, 2013, vol. 6 (2), pp. 13–26. DOI: 10.1016/j.procir.2013.03.002.
7. LotfiNeyestanak A.A., Daneshmand S. The effect of operational cutting parameters on Nitinol-60 in wire electrodischarge machining. *Advances in Materials Science and Engineering*, 2013, vol. 2013, pp. 1–6. DOI: 10.1155/2013/457186.
8. Sharma N., Raj T., Jangra K.K. Parameter optimization and experimental study on wire electrical discharge machining of porous Ni40Ti60 alloy. *Proceedings of the Institution of Mechanical Engineers, Part B: Journal of Engineering Manufacture*, 2013, vol. 231 (6), pp. 956–970. DOI: 10.1177/0954405415577710.
9. Safranski D., Dupont K., Gall K. Pseudoelastic NiTiNOL in orthopaedic applications. *Shape Memory and Superelasticity*, 2020, vol. 6, pp. 332–341. DOI: 10.1007/s40830-020-00294-y.
10. Rathod R., Kamble D., Ambhore N. Performance evaluation of electric discharge machining of titanium alloy – a review. *Journal of Engineering and Applied Science*, 2022, vol. 69 (1), pp. 1–19. DOI: 10.1186/s44147-022-00118-z.
11. Porwal R.K., Yadava V., Ramkumar J. Micro electrical discharge machining of micro-hole. *Advanced Science Engineering and Medicine*, 2020, vol. 12 (11), pp. 1335–1339. DOI: 10.1166/ asem.2020.2586.
12. Su X., Wang G., Yu J., Jiang F., Li J., Rong Y. Predictive model of milling force for complex profile milling. *The International Journal of Advanced Manufacturing Technology*, 2016, vol. 87, pp. 1653–1662. DOI: 10.1007/s00170-016-8589-1.
13. Gimadeev M.R., Nikitenko A.V., Berkun V.O. Influence of the sphero-cylindrical tool orientation angles on roughness under processing complex-profile surfaces. *Advanced Engineering Research*, 2023, vol. 23 (3), pp. 231–240. DOI: 10.23947/2687-1653-2023-23-3-231-240.
14. Sharakhovsky L.I., Marotta A., Essiptchouk A.M. Model of workpiece erosion for electrical discharge machining process. *Applied Surface Science*, 2006, vol. 253, pp. 797–804. DOI: 10.1016/j.apsusc.2006.01.013.
15. Barenji R.V., Pourasl H.H., Khojastehnezhad V.M. Electrical discharge machining of the AISI D6 tool steel: prediction and modeling of the material removal rate and tool wear ratio. *Precision Engineering*, 2016, vol. 45, pp. 435–444.
16. Klocke F., Schneider S., Ehle L., Meyer H., Hensgen L., Klink A. Investigations on surface integrity of heat treated 42CrMo4 (AISI 4140) processed by sinking EDM. *Procedia CIRP*, 2016, vol. 42, pp. 580–585. DOI: 10.1016/j.procir.2016.02.263.



17. Golabczak A., Konstantynowicz A., Golabczak M. Mathematical modelling of the physical phenomena in the interelectrode gap of the EDM process by means of cellular automata and field distribution equations. *Experimental and Numerical Investigation of Advanced Materials and Structures*, 2013, vol. 41, pp. 169–184. DOI: 10.1007/978-3-319-00506-5_11.
18. Kumar A., Mandal A., Dixit A.R., Mandal D.K. Quantitative analysis of bubble size and electrodes gap at different dielectric conditions in powder mixed EDM process. *The International Journal of Advanced Manufacturing Technology*, 2020, vol. 4 (1), pp. 1–11. DOI: 10.1007/s00170-020-05189-x.
19. Puri A.B., Bhattacharyya B. Modeling and analysis of white layer depth in a wire-cut EDM process through response surface methodology. *The International Journal of Advanced Manufacturing Technology*, 2005, vol. 25 (3), pp. 301–307. DOI: 10.1007/s00170-003-2045-8.
20. Ablyaz T.R., Zhurin A. Influence of wire-cut electrical discharge machining on surface quality. *Russian Engineering Research*, 2016, vol. 36 (2), pp. 156–158. DOI: 10.3103/S1068798X16020039.
21. Brown M., Wright D., Saoubi R.M., Gourlay J.M., Wallis M., Mantle A., Crawforth P., Ghadbeigi H. Destructive and non-destructive testing methods for characterization and detection of machining-induced white layer: a review paper. *CIRP Journal of Manufacturing Science and Technology*, 2018, vol. 23, pp. 39–53. DOI: 10.1016/j.cirpj.2018.10.001.

Conflicts of Interest

The authors declare no conflict of interest.

© 2025 The Authors. Published by Novosibirsk State Technical University. This is an open access article under the CC BY license (<http://creativecommons.org/licenses/by/4.0>).